

Influence of subsurface biosphere on geochemical fluxes from diffuse hydrothermal fluids

Scott D. Wankel^{1†}, Leonid N. Germanovich², Marvin D. Lilley³, Gence Genc², Christopher J. DiPerna¹, Alexander S. Bradley¹, Eric J. Olson³ and Peter R. Girguis^{1*}

Hydrothermal vents along mid-ocean systems host unique, highly productive biological communities, based on microbial chemoautotrophy, that thrive on the sulphur, metals, nitrogen and carbon emitted from the vents into the deep ocean. Geochemical studies of vents have centred on analyses of high-temperature, focused hydrothermal vents, which exhibit very high flow rates and are generally considered too hot for microbial life. Geochemical fluxes and metabolic activity associated with habitable, lower temperature diffuse fluids remain poorly constrained. As a result, little is known about the extent to which microbial communities, particularly in the subsurface, influence geochemical flux from more diffuse flows. Here, we estimate the net flux of methane, carbon dioxide and hydrogen from diffuse and focused hydrothermal vents along the Juan de Fuca ridge, using an *in situ* mass spectrometer and flowmeter. We show that geochemical flux from diffuse vents can equal or exceed that emanating from hot, focused vents. Notably, hydrogen concentrations in fluids emerging from diffuse vents are 50% to 80% lower than predicted. We attribute the loss of hydrogen in diffuse vent fluids to microbial consumption in the subsurface, and suggest that subsurface microbial communities can significantly influence hydrothermal geochemical fluxes to the deep ocean.

Hydrothermal vents along mid-ocean ridge systems are renowned for hosting unique, highly productive communities based on chemoautotrophic primary production¹. These vents are thought to play an important, yet largely unconstrained, role in global biogeochemical cycles of sulphur, metals, nitrogen and carbon. Recent studies estimate that hydrothermal fluid flow circulates the entire ocean volume through the crustal aquifer and out mid-ocean ridge vents every 70,000 to 200,000 years^{2–4}, underscoring the impact of hydrothermal circulation on ocean chemistry. Notably, these calculations are based largely on heat flux measurements and/or geochemical analyses from focused, high-temperature hydrothermal fluids and/or ridge flank aquifer formation pore fluids. Almost our entire understanding of inter- and intra-field fluid composition and variability^{5–10}, seafloor hydrogeology^{11–13} and subsurface microbial biogeochemistry and ecology^{14–19} stems from a limited number of analyses of discrete samples that have been analysed *ex situ*.

Although these studies have greatly furthered our understanding of hydrothermal vent hydrology and geochemistry, there are only a handful of studies that specifically characterize diffuse hydrothermal flow (referring hereafter to those low-temperature fluids that are proximal to and considered a dilution of high-temperature flows, for example, ref. 26). Data on the magnitude of diffuse flow and their role in geochemical fluxes to the global ocean are limited^{19,23–27}, although some reports have suggested that the geochemical influence of low-temperature diffuse flows to the global ocean might exceed that of high-temperature flows^{21,22}. Such slower flowing diffuse fluids have longer subsurface residence times, are rich in dissolved metals and volatiles, and generally exhibit lower temperatures, making them ‘hotspots’ for microbially mediated biogeochemical transformations. As such,

a more comprehensive and quantitative analysis of the potential magnitude of biogeochemical reactions in these widespread flow regimes is critical for constraining the role of the subsurface biosphere in global biogeochemical cycles.

Here we present results from submersible-based deployments of an *in situ* mass spectrometer and flowmeter to quantify geochemical fluxes from several low-temperature diffuse (as well as high-temperature focused) flow sites in hydrothermal vent fields along the Endeavour segment of the Juan de Fuca ridge. Deviations from conservative endmember mixing provide first-order *in situ* consumption estimates of H₂ in both diffuse and some focused flows, which we attribute to microbial activity in lower temperature fluids. These data provide one of the first direct broad-scale constraints on the role that diffuse flows play in geochemical flux to the ocean, the potential extent and magnitude of subsurface hydrogen oxidation, and the role that subsurface microbial activity may play in modification of hydrothermal vent geochemistry.

Flow velocities among diffuse and focused flow sites

Fluid flow measurements were made during four dives in a variety of flow regimes, including low-temperature diffuse flow environments as well as high-temperature ‘black smokers’ at a number of structures within the Main Endeavour and the Mothra fields on the Juan de Fuca ridge. Temperatures at the diffuse flow sites ranged from 9 to 81 °C, whereas focused vent orifices yielded temperatures ranging up to 321 °C (Table 1). Flow rates were determined by quantifying turbine rotation rate through video analysis (Table 2). Diffuse flow rates were determined in the Main Endeavour field and Mothra complex, and exhibited a range from ~1 to 10 cm s⁻¹. Linear flow velocities among the focused flows

¹Department of Organismic and Evolutionary Biology, Harvard University, Cambridge, Massachusetts 02138, USA, ²School of Civil and Environmental Engineering, Georgia Institute of Technology, Atlanta, Georgia 30332, USA, ³School of Oceanography, University of Washington, Seattle, Washington 98195, USA. [†]Present address: Department of Earth and Planetary Sciences, Harvard University, Cambridge, Massachusetts 02138, USA.

*e-mail: pgirguis@oeb.harvard.edu.

Table 1 | Hydrothermal fluid sample details from DSV *Alvin* dives 4418 to Faulty Towers (Mothra) and 4419 and 4420 to Dante (MEF) and Hulk (MEF) showing the type and temperature of fluid flow being sampled and the concentrations of CH₄, CO₂ and H₂ measured by the *in situ* mass spectrometer.

Vent field	Structure name	Site name	Fluid details		Concentrations (μM) from ISMS						
					CH ₄		CO ₂ (aq)		H ₂		
			Temp °C*	Type of Flow	Avg	S.d.	Avg	S.d.	Avg	S.d.	
Mothra	Faulty Towers	Worms 27-42	27-42	Diffuse	176	± 9	1,111	± 141	14	± 1.4	
Mothra	Faulty Towers	Hot Harold	307	Large focused	1,153	± 83	6,755	± 224	103	± 3.0	
Mothra	Faulty Towers	Worms 14-17	14-17	Diffuse	10	± 5	103	± 103	0.5	± 1.2	
Mothra	Faulty Towers	Diffuse 18-21	18-21	Diffuse	9	± 3	86	± 54	0.4	± 0.3	
Mothra	Faulty Towers	Base of Tower—Left	319	Large focused	881	± 39	5,124	± 345	64	± 3.3	
Mothra	Faulty Towers	Base of Tower—Right	321	Large focused	899	± 21	5,379	± 41	68	± 1.0	
Mothra	Faulty Towers	Diffuse 29-32	29-32	Diffuse	141	± 9	929	± 75	9	± 0.4	
Mothra	Faulty Towers	Camera 9-11	9-11	Diffuse	21	± 2	157	± 54	0.3	± 0.2	
Main Endeavour field	Dante	Dante 17.4	17.4	Diffuse	41	± 10	557	± 128	0.7	± 0.1	
Main Endeavour field	Dante	Dante 149	149	Small focused	448	± 37	6,017	± 380	45	± 3.5	
Main Endeavour field	Dante	Top of Dante	156	Small focused	438	± 23	5,957	± 155	20	± 2	
Main Endeavour field	Dante	Dante Worms	37.2	Diffuse	30	± 5	477	± 68	3	± 0.4	
Main Endeavour field	Dante	Dante BOSSa	108	Small focused	153	± 38	2,067	± 419	17	± 2.8	
Main Endeavour field	Hulk	Hulk Diffuse	10-12	Diffuse	8	± 4	114	± 64	0.0	± 0.2	
Main Endeavour field	Hulk	Hulk Chimney	190	Small focused	362	± 40	6,009	± 346	18	± 1.0	
Main Endeavour field	Dante	Dante BOSSb	86	Small focused	150	± 44	1,964	± 553	17	± 4.5	
Main Endeavour field	Dante	Dante BOSSc	52	Small focused	95	± 20	1,214	± 214	11	± 2.4	
Main Endeavour field	Hulk	Hulk Slurp1	9-17	Diffuse	29	± 8	482	± 168	1	± 0.4	
Main Endeavour field	Hulk	Hulk Slurp2	142-212	Small focused	569	± 73	8,029	± 479	30	± 3.8	
Main Endeavour field	Dante	Dante Slurp3	35-81	Diffuse	129	± 66	1,766	± 898	7	± 4.4	
Main Endeavour field	Dante	Dante Slurp4	12-16	Diffuse	48	± 3	699	± 35	0.6	± 0.3	
Average by type					Avg	S.d.	Avg	S.d.	Avg	S.d.	
					Diffuse	58	± 11	589	± 162	3	± 1
					Small focused	316	± 39	4465	± 364	22	± 3
					Large focused	978	± 47	5753	± 203	78	± 2

*Temperatures of small focused flows taken during dives 4419 and 4420 may be depressed owing to probe malfunction.

Table 2 | Mass fluxes of CH₄, CO₂(aq) and H₂ from individual focused flow structures.

Dive no.	Site name	Flow type	Flow rate			Mass fluxes for each structure (kmol yr ⁻¹)*		
			cm s ⁻¹	Area cm ²	m ³ d ⁻¹	CH ₄	CO ₂ (aq)	H ₂
4418	Hot Harold	Large focused	35.5	150	460 ± 230	194 ± 98	1130 ± 566	17.2 ± 8.6
4418	Base of Tower—Left	Large focused	35.5	150	460 ± 230	148 ± 74	860 ± 434	10.7 ± 5.4
4418	Base of Tower—Right	Large focused	35.5	250	767 ± 383	252 ± 126	1,510 ± 755	19.2 ± 9.6
4419	Dante 149	Small focused	5.0	49	21 ± 11	3.5 ± 1.8	46 ± 23.4	0.35 ± 0.18
4419	Top of Dante	Small focused	3.9	13	4.2 ± 2	0.7 ± 0.3	9.2 ± 4.6	0.03 ± 0.02
4419	Dante BOSSa	Small focused	7.3	7.3	4.6 ± 2	0.3 ± 0.1	3.5 ± 1.9	0.03 ± 0.02
4419	Hulk Chimney	Small focused	6.3	14.3	7.8 ± 4	1.0 ± 0.5	17 ± 8.6	0.05 ± 0.03
4420	Dante BOSSb	Small focused	7.3	7.3	4.6 ± 2	0.3 ± 0.1	3.3 ± 1.9	0.03 ± 0.02
4420	Dante BOSSc	Small focused	7.3	7.3	4.6 ± 2	0.2 ± 0.1	2.0 ± 1.1	0.02 ± 0.01
4420	Hulk Slurp2	Small focused	8.2	5.0	3.5 ± 2	0.7 ± 0.4	10 ± 5.2	0.04 ± 0.02
Large focused						198 ± 99.4	1,170 ± 585	16 ± 7.9
Small focused						0.9 ± 0.5	13 ± 6.7	0.08 ± 0.04

*Error estimates for geochemical fluxes incorporate three sources, in order of increasing contribution: uncertainty of the *in situ* mass spectrometer concentration measurements, uncertainty owing to turbulent variations of the volatile signal observed while sampling and uncertainty in the measurement of linear flow velocity. Mean values for small and large vent structures are given.

ranged from 3.9 cm s⁻¹ at the Top of Dante up to 35.5 cm s⁻¹ at the main Tower Vent at Mothra (Table 2) with co-registered fluid temperatures from 52 to 321 °C, respectively. Linear flow velocities were generally much higher at the black smokers than in the more diffuse regions. Digital estimates of focused flow orifice sizes (using analytical graphics software together with the calibrated laser sights

on the submersible camera) allowed calculation of fluid discharge for each point of focused flow (Table 2). Estimates of fluid discharge ranged from as low as 3.5 m³ d⁻¹ (a small focused flow called 'Slurp 2' at Hulk in the Main Endeavour field) up to as high as 767 m³ d⁻¹ (the primary focused flow on the 'Main Tower Vent' at Faulty Towers in the Mothra field).

Volatile concentrations at diffuse and focused flow sites

During three consecutive dives to the Mothra and Main Endeavour vent fields, we measured substantial differences in fluid chemical composition (Table 1) among the three major structures sampled (Faulty Towers, Hulk and Dante). Figure 1 is a time series from dive 4418 that illustrates the temporal variability in H_2 , CH_4 and $\text{CO}_{2(\text{aq})}$ concentrations observed among the different sites during the course of a dive. Over the course of all three dives, observed concentrations of H_2 , CH_4 , and $\text{CO}_{2(\text{aq})}$ ranged from 0.3 to 103 μM , 8 to 1,153 μM and 86 to 8,029 μM , respectively, across all sites (Table 1). The low velocities of diffuse flow allow pronounced and variable mixing with sea water and, accordingly, lead to larger variability in both temperature and fluid chemistry. Figure 2 illustrates the composition of fluids sampled during each dive over a full span of sampling conditions, ranging from turbulent low-temperature diffuse fluids to direct sampling of high-temperature black smokers. Conservative mixing lines (seen as curves on log–log plots) depict chemical concentrations that would be expected solely as a result of physical mixing of two endmember fluids (for example, background sea water and vent fluid). The chemical composition of ambient sea water was used as the seawater endmember (defined as 31 μM $\text{CO}_{2(\text{aq})}$ and 1 nM CH_4 and H_2), whereas the composition of the highest observed temperature fluids was used as the vent fluid endmember. Endmember $\text{CO}_{2(\text{aq})}$ concentrations in focused flows were substantially elevated above sea water at both vent fields (5.4–8.0 mM), consistent with dissolved inorganic carbon (DIC) concentrations observed in gastight samples from the same structure (Supplementary Table S2). At the pH observed at Hulk and Dante (Hulk = 4.35; Dante = 5.3; ref. 28) $\text{CO}_{2(\text{aq})}$ represents >95% of the total DIC pool. With respect to H_2 and CH_4 , concentrations were also consistent with independent gastight samples (Supplementary Table S2). For example, the ‘Hot Harold’ orifice at Faulty Towers showed substantially higher H_2 ($103 \pm 3 \mu\text{M}$) and CH_4 ($1,153 \pm 83 \mu\text{M}$) than the Dante orifice in the Main Endeavour field ($\text{H}_2 = 45 \pm 3.5 \mu\text{M}$; $\text{CH}_4 \sim 448 \pm 37 \mu\text{M}$) and Hulk ($\text{H}_2 = 30 \pm 3.8 \mu\text{M}$; $\text{CH}_4 = 569 \pm 73 \mu\text{M}$; Table 1). These observations are also consistent with decreases in H_2 , CH_4 and $\text{CO}_{2(\text{aq})}$ concentrations along the Main Endeavour field in the wake of the 1999 eruption^{5,29,30}.

Differences were also observed in fluid composition among the structures and orifices within the same field (Fig. 2). Some structures, such as Hulk and Dante at the Main Endeavour field, exhibited striking differences in mixing lines despite their physical proximity, demonstrating that these structures are allied to different subsurface upflow zones³¹. We also observed substantial variations in volatile composition on a single vent structure. For example, the Main Tower Vent at Faulty Towers in the Mothra field contained less H_2 than the fluids at Hot Harold, despite being within ~ 15 m of one another (Fig. 2). This underscores the spatial heterogeneity in the processes affecting the composition of hydrothermal fluids, such as mineral precipitation and phase separation at high temperatures^{5,6,20}. Even when active vent orifices are separated by only tens of metres, we observed that higher temperature fluids do not always correspond to higher volatile concentrations. Such heterogeneity was most clearly observed at Dante, where four of the sites (‘Top of Dante’ and ‘Dante Diffuse 17.4’ during dive 4419 and ‘Slurp3’ and ‘Slurp4’ during dive 4420) deviated from conservative mixing, suggesting reactions that are consuming H_2 relative to $\text{CO}_{2(\text{aq})}$ (Fig. 2e). Nevertheless, the highest temperature fluids sampled at Dante (the ‘Top of Dante’ and ‘Slurp3’ sites) showed striking similarities in chemical composition to those at Hulk, as evidenced by the resemblance to the Hulk–seawater mixing line (Fig. 2), and reflect an apparently more complex subsurface plumbing network between Dante and Hulk³¹.

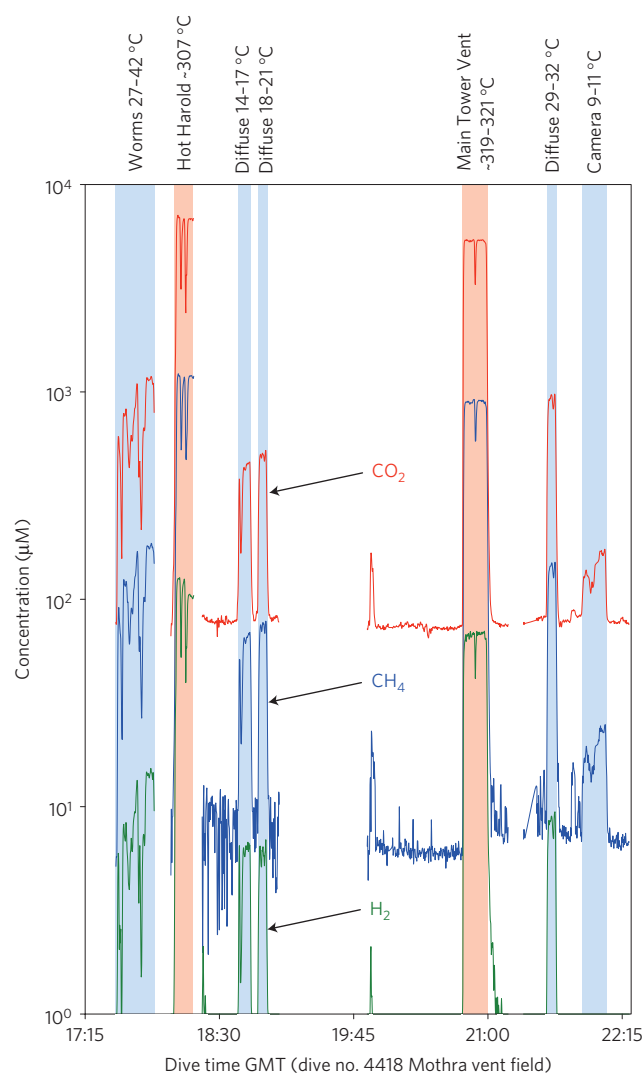


Figure 1 | Time-series of selected volatile concentrations from survey of the Faulty Towers vent structure in Mothra hydrothermal vent field.

Measurements of ion intensities were made by the *in situ* mass spectrometer (ISMS) during dive AD4418 on 14 July 2008. ISMS ion intensities were converted to concentrations based on previous calibration (see Methods). Signals shown include molecular H_2 (m/z 2), CH_4 (m/z 15) and $\text{CO}_{2(\text{aq})}$ (m/z 44). Sample fluids were continuously delivered past the membrane inlet of the ISMS via a sampling wand periodically placed into environments/fluids of interest including focused flow structures and areas of more diffuse flows replete with tubeworm aggregations and microbial mats.

Geochemical fluxes among diffuse and focused flows

Using video-assisted estimation of the cross sectional area of each orifice, together with flow velocity measurements and the direct concentration measurements with the *in situ* mass spectrometer (ISMS), we calculated geochemical fluxes from the sampling sites where both instruments were deployed (Tables 2, 3). Among the focused flows, fluxes of H_2 , CH_4 and $\text{CO}_{2(\text{aq})}$ from individual orifices ranged from 0.02 to 19.2 kmol yr^{-1} , 0.2 to 252 kmol yr^{-1} , and 2 to 1,510 kmol yr^{-1} , respectively, with the largest fluxes associated with the larger focused flow orifices (Table 2). To compare the focused flow values with diffuse flows, we normalize the H_2 , CH_4 and $\text{CO}_{2(\text{aq})}$ fluxes by area (Table 3), yielding average values of ~ 900 , 11,000 and 64,300 $\text{kmol m}^{-2} \text{yr}^{-1}$ for large and ~ 40 , 600 and 8,800 $\text{kmol m}^{-2} \text{yr}^{-1}$ for small focused flows, respectively. Area normalized fluxes from the orifices of smaller sulphides were on

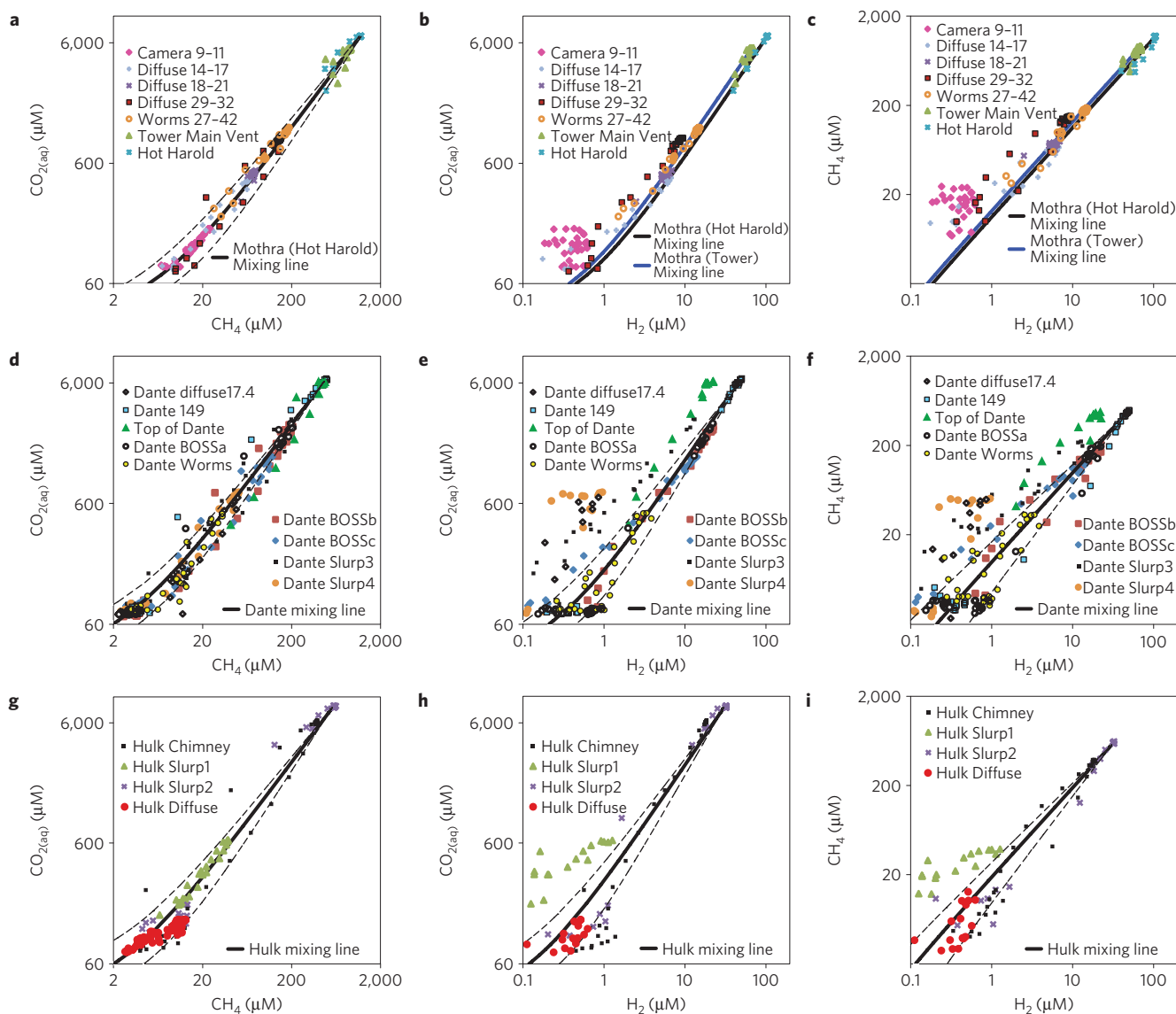


Figure 2 | Mixing diagrams of $\text{CO}_2(\text{aq})$, CH_4 and H_2 from surveys of Faulty Towers (Mothra), Dante (MEF) and Hulk (MEF) vent structures.

Concentrations plotted against one another for illustration of relative behaviour. Solid lines are conservative two-endmember mixing lines (dashed lines represent estimates of error) calculated based on compositions of background sea water and those observed in the hottest sampled vent fluid. Faulty Towers (a–c), Dante (d–f), Hulk (g–i). Data for Dante and Hulk come from two independent ISMS deployments, confirming the robustness of the observed mixing trends. Several sites (at Dante and Hulk) exhibited substantial H_2 deficits implying an important role of subsurface biosphere in the oxidation of H_2 .

average only 5–14% of those from larger structures, owing mostly to the much higher flow velocities ($\sim \times 10$) from the larger orifices.

So far, the relative importance of fluxes from diffuse venting fluids has been difficult to characterize. Using quantitative, imagery-based estimates of the areal coverage of diffuse flow (based on the presence of microbial mat and/or macrofaunal growth) on an active sulphide ('Finn' in the Mothra field), together with the ISMS data and measurements of diffuse linear flow velocities, we determined the relative contributions of geochemical flux from diffuse flows (Table 3). Using a conservative mean value of 5 cm s^{-1} for linear flow velocity (previous estimates range 4 to 18 cm s^{-1} (refs 22,32–34) from sites at the Main Endeavour field, as well as other sites), we calculate average areal fluxes of H_2 , CH_4 and $\text{CO}_2(\text{aq})$ from diffuse flows to be 5, 92 and $940 \text{ kmol m}^{-2} \text{ yr}^{-1}$ respectively (Table 3). Although these areal fluxes are considerably lower than those from focused flows, the areal extent of diffuse flow is considerably greater (>100 times greater for 'Finn'). On Finn the diffusive fluxes of H_2 , CH_4 and $\text{CO}_2(\text{aq})$ would be 21, 380

and $3,600 \text{ kmol yr}^{-1}$, whereas those from the focused flow at the main orifice of Finn would be 30, 380 and $2,200 \text{ kmol yr}^{-1}$. Hence, total diffuse CH_4 flux was approximately equal to the focused flow flux out the top of the structure, whereas $\text{CO}_2(\text{aq})$ fluxes were $\sim 50\%$ higher from low-temperature diffuse flows and H_2 fluxes were $\sim 50\%$ lower from the diffuse flows. These data, based on a conservative fluid flow velocity in diffuse flows, suggest that geochemical flux from low-temperature diffuse flow areas spatially associated with active venting (on Juan de Fuca ridge) equals and probably exceeds geochemical flux from larger focused flow structures (depending on actual concentration, flow rate and areal expression). These data underscore the relative importance of diffuse flows in geochemical flux from comparable hydrothermal vents to the deep ocean, and are supported by heat flux-based estimates of fluid contribution from diffuse flow³⁵. In light of the diverse structural topography and hydrology among vents, future studies should employ similar approaches to better constrain the role of diffuse flow in geochemical flux at slow- and fast-spreading centres.

Table 3 | Area normalized fluxes of large focused (for example, central black smoker), small focused flows (for example, secondary flow structures) and diffuse flow (for example, beehives, tubeworm bushes, porous sulphides, and so on). Error estimates as in Table 2.

Dive no.	Site name	Flow type	Areal flux ($\text{kmol m}^{-2} \text{yr}^{-1}$)		
			CH_4	$\text{CO}_{2(\text{aq})}$	H_2
4418	Worms 27–42	Diffuse	280 ± 140	1,800 ± 930	22 ± 11
4418	Hot Harold	Large focused	12,900 ± 6,520	75,300 ± 37,700	1,150 ± 580
4418	Worms 14–17	Diffuse	16 ± 11	160 ± 180	0.7 ± 2.0
4418	Diffuse 18–21	Diffuse	14 ± 8	140 ± 110	0.6 ± 0.6
4418	Base of Tower—Left	Large focused	9,860 ± 4,950	57,300 ± 28,900	712 ± 360
4418	Base of Tower—Right	Large focused	10,100 ± 5,060	60,400 ± 30,200	766 ± 380
4418	Diffuse 29–32	Diffuse	220 ± 110	1,500 ± 760	13 ± 6.7
4418	Camera 9–11	Diffuse	34 ± 17	250 ± 150	0.5 ± 0.4
4419	Dante 17.4	Diffuse	64 ± 35	880 ± 480	1.0 ± 0.6
4419	Dante 149	Small focused	707 ± 360	9,500 ± 4,800	72 ± 36
4419	Top of Dante	Small focused	539 ± 270	7,300 ± 3,700	24 ± 12
4419	Dante Worms	Diffuse	48 ± 25	750 ± 390	5.4 ± 2.8
4419	Dante BOSSa	Small focused	350 ± 200	4,800 ± 2,600	39 ± 21
4419	Hulk Diffuse	Diffuse	13 ± 8	180 ± 130	0.0 ± 0.3
4419	Hulk Chimney	Small focused	720 ± 370	11,900 ± 6,000	35 ± 18
4420	Dante BOSSb	Small focused	350 ± 200	4,500 ± 2,600	38 ± 22
4420	Dante BOSSc	Small focused	220 ± 120	2,800 ± 1,500	24 ± 13
4420	Hulk Slurp1	Diffuse	45 ± 26	760 ± 460	0.9 ± 0.8
4420	Hulk Slurp2	Small focused	1,500 ± 770	21,000 ± 10,600	78 ± 40
4420	Dante Slurp3	Diffuse	200 ± 140	2,800 ± 2,000	11 ± 9.0
4420	Dante Slurp4	Diffuse	75 ± 38	1,100 ± 550	0.9 ± 0.6
		Large focused	11,000 ± 5,510	64,300 ± 32,300	876 ± 440
		Small focused	630 ± 330	8,800 ± 4,500	44 ± 23
		Diffuse	92 ± 51	940 ± 560	5.1 ± 3.2
			0.057	0.137	0.051

Estimates of subsurface microbial hydrogen consumption

In our data, we frequently observe depletion of H_2 relative to $\text{CO}_{2(\text{aq})}$ at many lower temperature diffuse flows, as well as several small focused flows (Fig. 2). To evaluate non-conservative behaviour of H_2 in diffuse and focused flows, herein we use $\text{CO}_{2(\text{aq})}$ as a proxy for a conservative tracer in two-endmember mixing, which has been previously demonstrated as reflective of simple two-endmember mixing in recent studies^{27,36}. $\text{CO}_{2(\text{aq})}$ provided the most robust ISMS signal across all sampling sites and is mixed nearly linearly under these physicochemical conditions (range of temperature and pH; ref. 37). Although seemingly counterintuitive in light of biological processes that could influence DIC via chemoautotrophy, methanogenesis or respiration, the high concentrations of DIC in both sea water and vent fluid (2.3 mM DIC in sea water and ~7 mM DIC in vent fluids) and the substantial flow rates (4,000–400,000 L d^{-1}) result in very high fluxes (on the order of 10–10,000 $\text{kmol m}^{-2} \text{yr}^{-1}$), which biological processes are unlikely to substantially influence (at least within resolution of the data presented here). As an example, the highest measured deep-sea carbon fixation rates so far have been observed in *Ridgeia piscesae* and *Riftia pachyptila*, vent tubeworms that host chemoautotrophic symbionts. These symbioses can fix DIC at rates of up to 4.4 $\text{mol m}^{-2} \text{yr}^{-1}$ (refs 38,39), which, within all the diffuse flows measured herein, would at most influence the DIC flux by ~0.03%. Although variations in deep subsurface microbial activity may influence the DIC pool on broader spatial scales (for example, through methanogenesis or heterotrophy), the proximity of the diffuse and focused flows considered here allow the assumption that low temperature diffuse fluids are a dilution of the high-temperature ‘parent’ fluid and, thus, that modifications to conservative mixing are localized in the shallow subsurface.

Using the ISMS measurements and the calculated fluxes, we estimated an areal loss rate (see Supplementary Information for details) for each sampling site based on the difference between the actual H_2 flux and that predicted from the mixing line for eight sites. As a result of some uncertainty in subsurface hydrologic connectivity (see above), comparisons were made with the different endmember compositions (for example, some fluids issuing from Dante may actually more appropriately be compared with a Hulk fluid endmember (Fig. 2)). At sites where deviations were observed, areal H_2 loss rates ranged from 2,000 to 31,200 $\text{mol m}^{-2} \text{yr}^{-1}$ (Table 4). In many cases >50% of the expected H_2 was removed before exiting the vent orifice. In particular, at the diffuse- and small focused-flow sites, where surficial temperatures were below 100 °C, H_2 removal was often >80% (Table 4). Assuming that the bulk of the high-temperature production of H_2 through mineral alteration takes place in the deeper, high-temperature areas below the sea floor then, to first order, we would expect spatially associated fluids expelled on or around the same structure to be compositionally similar. Thus, although deviations between the compositions of larger, vigorously flowing orifices on the same structure can be indicative of variation in fluid source and the degree of fluid–basalt interactions (which act to produce H_2) deep below the sulphide structure, the substantially greater loss of hydrogen in lower temperature, diffuse flow milieus strongly implicates subsurface biological activity in the loss of hydrogen. Although we cannot neglect the influence of mineralization on the production of H_2 relative to $\text{CO}_{2(\text{aq})}$, the observed H_2 deficits represent a conservative estimate of H_2 consumption, likely biological in nature, during transport through the subsurface or in near-floor mixing zones.

Moreover, greater proportional H_2 deficits were observed at sites on horizontal surfaces near the base of large structures

Table 4 | Areally expressed hydrogen deficits in diffuse fluids based on comparison with two potential vent endmembers.

Dive	Site	Temp °C	Endmember	% lost*	Loss rate kmol m ⁻² yr ⁻¹
4418	Worms 27–42	27–42	Hot Harold	16%	4.1
			Tower	1%	0.2
4418	Diffuse 29–32	29–32	Hot Harold	38%	8.2
			Tower	24%	4.3
4418	Camera 9–11	9–11	Hot Harold	84%	2.6
			Tower	81%	2.0
4419	Dante 17.4	17	Dante 149	84%	5.3
			Hulk Slurp2	67%	3.4
4419	Top of Dante	156	Dante 149	56%	31.2
			Hulk Slurp2	12%	7.1
4420	Dante Slurp3	35–81	Dante 149	46%	9.5
			Hulk Slurp2	–9%	–1.5
4420	Dante Slurp4	12–16	Dante 149	88%	7.0
			Hulk Slurp2	77%	5.0
4420	Hulk Slurp1	9–17	Hulk Slurp2	67%	2.9

For example, several fluids at Dante seemed to be more closely related to chemical composition of Hulk fluids. At low temperature diffuse flow sites, hydrogen was often almost completely consumed before the fluid emanated from the structure, strongly implicating the role of biological oxidation by the subsurface. *Calculated as Measured [H₂]/Expected [H₂].

(for example, Dante 17.4 and DanteSlurp4; Table 4) as compared with those low-temperature sites directly on the side of large structures (for example, Worms 27–42 and Diffuse 29–32; Table 4), implying greater loss with longer subsurface residence time. H₂ oxidation under hydrothermal vent conditions is a more thermodynamically favourable source of energy than H₂S oxidation⁴⁰, and thermophilic H₂ oxidizing bacteria are known to be ubiquitous in hydrothermal systems^{15,41,42}. Hydrogen-dependent microbial reduction of sulphur, iron, manganese or even nitrate may also be occurring⁴⁰, and future studies should aim to better resolve the relative contribution of each particular metabolism to hydrogen oxidation. H₂ consumption has already been qualitatively associated with methanogenesis in some diffuse flow fluids^{9,23,26}. It is probable that the methane in these diffuse flows could be derived from H₂ consumption by methanogens. Although our data on CH₄ suggest that methanogenesis is prominent at some sites (as evidenced by data falling to the right of the CH₄–CO_{2(aq)} mixing line as in Fig. 2d,g), CH₄ concentrations at all sites were too high to be able to distinguish any stoichiometric relationship between hydrogen consumption and methanogenesis, or for that matter to make any inferences about subsurface methanotrophy. Future co-registered examination of volatile concentrations, stable isotopic composition and/or targeted microbial activity would be better suited to establishing these specific relationships.

Our understanding of marine biogeochemistry has improved dramatically in recent years, in large part owing to our ability to make measurements that directly connect microbial activity to geochemical fluxes. Until now, technical restrictions have limited these measurements to the water column and sediment environments. This report demonstrates how development of a new *in situ* technology can circumvent these constraints and allow the direct examination of subsurface biogeochemistry, including determination of the nature and extent of microbial influence on geochemical fluxes from hydrothermal vents. Recent studies of deep subsurface sediments and aquifers have suggested the existence of a tremendous subsurface biosphere, the metabolic activity of which remains enigmatic. Together, the data herein offer one of the first glimpses into microbial subsurface metabolism, provide first order constraints on the degree to which the subsurface biosphere can influence biogeochemical cycles, and further underscore the need for continued characterization of diffuse flow regimes. Future efforts should be aimed at using similar approaches in other systems, for example serpentinization-dominated systems, and

advancing *in situ* analytical tools to interrogate more difficult settings such as hydrothermal recharge zones.

Methods

Site description. The Endeavour segment of the Juan de Fuca ridge is a tectonically controlled, seismically active, intermediate spreading centre hosting five major hydrothermal vent fields, the fluid geochemistry of which is influenced by magmatic processes (for example, CO₂, He, H₂), hydrothermal alteration (for example, H₂) and interaction with organic-rich sediments during hydrologic recharge (for example, CO₂, CH₄, NH₄⁺; refs 5,6,29,43).

Calibration of the *in situ* mass spectrometer. Benchtop calibrations were performed using high-pressure pumps (Beckman-Coulter, Fullerton, CA) to deliver calibrated solutions (typically, sea water equilibrated with known mixtures of gases) past the membrane inlet over a range of flow rates, temperatures and hydrostatic pressures. Temperature of the sample fluid and membrane inlet was controlled by immersion in a temperature-controlled bath (±0.1 °C). Hydrostatic pressure was monitored with high-pressure gauges and was controlled by a back-pressure regulator (StraVal Valve, Garfield, NJ). Independent analyses of dissolved gases were performed with a gas chromatograph (HP 5890) with an injection port designed for degassing seawater samples⁴⁴. Relative changes in the ion intensity within the mass spectrometer are assumed to be linearly proportional to changes in the permeation of gas through the membrane, which is in turn linearly proportional to concentration, as described by Fick's law⁴⁵. The steady-state flux of a gas permeating through a membrane is the product of the permeability coefficient, the membrane surface area and the concentration gradient between both sides of the membrane (because the inner surface of the membrane is under high vacuum, the concentration of gases on the inside relative to the outside is very small and can be neglected). In such high-pressure applications, permeation through polymeric membranes can be influenced by changes in hydrostatic pressure owing to compression, swelling, competitive sorption and changes in geometry^{45,46}. Thus, changes in hydrostatic pressure can influence permeability and lead to artefactual changes in the magnitude of ion intensity independent of concentration. Nevertheless, during multiple laboratory calibrations, we found Teflon AF membranes to be extremely resistant to change under large ranges of hydrostatic pressure, with relative changes in ion intensity always <10%, which is consistent with a previous material characterization study⁴⁷.

Environmental sampling. *In situ* vent fluid sampling was carried out on three dives with the DSV *Alvin* (Supplementary Table S1) during July 2008 (Dives 4418, 4419, and 4420). A submersible pumping system (Seabird Electronics, Seattle, WA) was used to deliver sample water from a titanium sampling wand to the membrane inlet through 1/4" polyurethane tubing. Sampling was carried out until steady state conditions were reached, as monitored in real time from within the submersible via the RGA software (v3.0, SRS). Concentrations were calculated based on empirically derived calibrations (Supplementary Fig. S1) and average signal response during steady-state sampling. Fluid temperature at the tip of the sampling wand was monitored via an inline J-type thermocouple read wirelessly through an inductively coupled link. Transport through the 1/4" tubing (surrounded by ambient sea water at ~1.8 °C) allowed fluids to be radiatively cooled before arrival at the membrane surface. Data from temperature data-loggers inside the membrane inlet verified

that temperatures remained steady ($\pm 0.1^\circ\text{C}$) during ISMS measurements and small corrections for changes in inlet temperature were applied (Supplementary Fig. S2) by using ion intensity of water (m/z 18) as a proxy for temperature⁴⁸. Independent gastight sample bottles⁴⁹ were also used to collect vent fluid for cross-calibration of the ISMS data (Supplementary Table S2). Over the course of the three dives, more than 2,400,000 data points were collected during $\sim 3,500$ scans of atomic mass ranging from m/z 2 to m/z 70.

Validation of environmental measurements. Five high-temperature endmember samples were collected via gastight samplers concurrently with ISMS measurements, and correlate well with the ISMS concentration data for H_2 and CH_4 (Supplementary Table S2). As a result of the absence of independent pH or alkalinity measurements, ISMS dissolved CO_2 measurements, referred to as $\text{CO}_{2(\text{aq})}$, cannot be compared with gastight CO_2 measurements, as these are acidified during processing to yield total dissolved inorganic carbon (DIC). ISMS sampled fluids having lower pH contain increasingly higher $\text{CO}_{2(\text{aq})}$, elevating the response at m/z 44 independent of total DIC. Nevertheless, the response of m/z 44 directly reflects the mixing of sea water with vent fluid and is used here with other gases for estimating deviations from conservative mixing.

Fluid flow measurements. Linear flow velocities were measured by the use of a positive displacement flowmeter⁵⁰ having a rotor with five or seven precision-fitted cups (Supplementary Fig. S3), with a known and fixed volume being displaced between the rotor-cups. Through empirical calibration, the rotation rate of the rotors was determined to be linearly proportional—over the range of velocities and flow rates presented here—to the linear flow velocity entrained by a circular cone placed directly above the flow being measured (Supplementary Fig. S3). Measurements were made at a variety of sites, including large and small focused flow structures as well as several diffuse flow sites. Rotation rates were determined based on reviewing at least five minutes of high-definition video.

Received 23 August 2010; accepted 16 May 2011; published online 19 June 2011

References

- Fisher, C. R. Jr, Takai, K. & Le Bris, N. Hydrothermal vent ecosystems. *Oceanography* **20**, 18–27 (2007).
- Johnson, H. P. & Pruis, M. J. Fluxes of fluid and heat from the oceanic crustal reservoir. *Earth Planet. Sci. Lett.* **216**, 565–574 (2003).
- Mottl, M. J. in *Energy and Mass Transfer in Marine Hydrothermal Systems* (eds Halbach, P., Tunnicliffe, V. & Hein, J.) 271–286 (Dahlem Univ. Press, 2003).
- Wheat, C. G., McManus, J., Mottl, M. J. & Giambalvo, E. Oceanic phosphorus imbalance: Magnitude of the mid-ocean ridge flank hydrothermal sink. *Geophys. Res. Lett.* **30**, 1895–1899 (2003).
- Lilley, M. D., Butterfield, D. A., Lupton, J. E. & Olson, E. J. Magmatic events can produce rapid changes in hydrothermal vent chemistry. *Nature* **422**, 878–881 (2003).
- Lilley, M. D. *et al.* Anomalous CH_4 and NH_4^+ concentrations at an unsedimented mid-ocean-ridge hydrothermal system. *Nature* **364**, 45–47 (1993).
- Tivey, M. K. Generation of seafloor hydrothermal vent fluids and associated mineral deposits. *Oceanography* **20**, 50–65 (2007).
- Tivey, M. K., Humphris, S. E., Thompson, G., Hannington, M. D. & Rona, P. A. Deducing patterns of fluid flow and mixing within the TAG active hydrothermal mound using mineralogical and geochemical data. *J. Geophys. Res.* **100**, 12527–12555 (1995).
- Von Damm, K. L. & Lilley, M. D. in *The Subfloor Biosphere at Mid-Ocean Ridges* (eds Wilcock, W. S. D., DeLong, E. F., Kelley, D. S., Baross, J. A. & Cary, S. C.) 245–268 (American Geophysical Union, 2004).
- Von Damm, K. L. *et al.* Evolution of East Pacific Rise hydrothermal vent fluids following a volcanic eruption. *Nature* **375**, 47–50 (1995).
- Wheat, C. G. *et al.* Heat and fluid flow through a basaltic outcrop on a ridge flank. *Geochem. Geophys. Geosyst.* **5**, Q12006 (2004).
- Hutnak, M. *et al.* Large heat and fluid fluxes driven through mid-plate outcrops on ocean crust. *Nature Geosci.* **1**, 611–614 (2008).
- Fisher, A. T. *et al.* Hydrothermal Vent recharge and discharge across 50 km guided by seamounts on a young ridge flank. *Nature* **421**, 618–621 (2003).
- Huber, J. A., Butterfield, D. A. & Baross, J. A. Temporal changes in archaeal diversity and chemistry in a mid-ocean ridge subsurface habitat. *Appl. Environ. Microbiol.* **68**, 1585–1594 (2002).
- Chapelle, F. H. *et al.* A hydrogen-based subsurface microbial community dominated by methanogens. *Nature* **415**, 312–315 (2002).
- Summit, M. & Baross, J. A. A novel microbial habitat in the mid-ocean ridge subsurface. *Proc. Natl Acad. Sci. USA* **98**, 2158–2163 (2001).
- Sogin, M. L. *et al.* Microbial diversity in the deep sea and the underexplored ‘rare biosphere’. *Proc. Natl Acad. Sci. USA* **103**, 12115–12120 (2006).
- Huber, J. A., Butterfield, D. A., Johnson, H. P. & Baross, J. A. Microbial life in ridge flank crustal fluids. *Environ. Microbiol.* **8**, 88–99 (2006).
- Edwards, K. J., Bach, W. & McCollom, T. M. Geomicrobiology in oceanography: Microbe-mineral interactions at and below the seafloor. *Trends Microbiol.* **13**, 449–456 (2005).
- Butterfield, D. A. *et al.* Gradients in the composition of hydrothermal fluids from the Endeavor segment vent field: Phase separation and brine loss. *J. Geophys. Res.* **99**, 9561–9583 (1994).
- Elderfield, H. & Schultz, A. Mid-ocean ridge hydrothermal fluxes and the chemical composition of the ocean. *Annu. Rev. Earth Planet. Sci.* **24**, 191–224 (1996).
- Schultz, A., Delaney, J. R. & McDuff, R. E. On the partitioning of heat flux between diffuse and point source seafloor venting. *J. Geophys. Res.* **97**, 12299–12315 (1992).
- Butterfield, D. A. *et al.* in *The Subseafloor Biosphere at Mid-Ocean Ridges* (eds Wilcock, W. S. D., DeLong, E. F., Kelley, D. S., Baross, J. A. & Cary, S. C.) 269–289 (American Geophysical Union, 2004).
- Johnson, K. S., Beehler, C. L., Sakamoto-Arnold, C. M. & Childress, J. J. *In situ* measurements of chemical distributions in a deep-sea hydrothermal vent field. *Science* **213**, 1139–1141 (1986).
- Le Bris, N., Govenar, B., Le Gall, C. & Fisher, C. R. Jr Variability of physico-chemical conditions in $9^\circ 50'$ N EPR diffuse flow vent habitats. *Mar. Chem.* **98**, 167–182 (2006).
- Proskurowski, G., Lilley, M. D. & Olson, E. J. Stable isotopic evidence in support of active microbial methane cycling in low-temperature diffuse flow vents at $9^\circ 50'$ N East Pacific Rise. *Geochim. Cosmochim. Acta* **72**, 2005–2023 (2008).
- Walker, B. D., McCarthy, M. D., Fisher, A. T. & Guilderson, T. P. Dissolved inorganic carbon isotopic composition of low-temperature axial and ridge-flank hydrothermal fluids of the Juan de Fuca Ridge. *Mar. Chem.* **108**, 123–136 (2008).
- Ding, K. *et al.* The *in situ* pH of hydrothermal fluids at mid-ocean ridges. *Earth Planet. Sci. Lett.* **237**, 167–174 (2005).
- Seewald, J. S., Cruse, A. & Saccocia, P. Aqueous volatiles in hydrothermal fluids from the Main Endeavor Field, northern Juan de Fuca Ridge: Temporal variability following earthquake activity. *Earth Planet. Sci. Lett.* **216**, 575–590 (2003).
- Seyfried, W. E. Jr, Seewald, J. S., Berndt, M. E., Ding, K. & Foustoukos, D. I. Chemistry of hydrothermal vent fluids from the Main Endeavor Field, northern Juan de Fuca Ridge: Geochemical controls in the aftermath of June 1999 seismic events. *J. Geophys. Res.* **108**, 2429–2452 (2003).
- Tivey, M. A. & Johnson, H. P. Crustal magnetization reveals subsurface structure of Juan de Fuca Ridge hydrothermal vent fields. *Geology* **30**, 979–982 (2002).
- Sarrazin, J. *et al.* A dual sensor device to estimate fluid flow velocity at diffuse hydrothermal vents. *Deep-Sea Res. I* **56**, 2065–2074 (2009).
- Ramondenc, P., Germanovich, L. N., Von Damm, K. L. & Lowell, R. P. The first measurements of hydrothermal heat output at $9^\circ 50'$ N, East Pacific Rise. *Earth Planet. Sci. Lett.* **245**, 487–497 (2006).
- Rona, P. A. & Trivett, D. Discrete and diffuse heat transfer at Ashes vent field, Axial Volcano, Juan de Fuca Ridge. *Earth Planet. Sci. Lett.* **109**, 57–71 (1992).
- Veirs, S. R., McDuff, R. E. & Stahr, F. R. Magnitude and variance of near-bottom horizontal heat flux at the Main Endeavor hydrothermal vent field. *Geochem. Geophys. Geosyst.* **7**, Q02004 (2006).
- Foustoukos, D. I., Pester, N. J., Ding, K. & Seyfried, C. F. Dissolved carbon species in associated diffuse and focused flow hydrothermal vents at the Main Endeavor Field, Juan de Fuca Ridge: Phase equilibria and kinetic constraints. *Geochem. Geophys. Geosyst.* **10**, Q10003 (2009).
- Zeebe, R. E. & Wolf-Gladrow, D. *CO₂ in Seawater: Equilibrium, Kinetics, Isotopes* (Elsevier, 2001).
- Girguis, P. R. & Childress, J. J. Metabolite uptake, stoichiometry and chemoautotrophic function of the hydrothermal vent tubeworm *Riftia pachyptila*: Responses to environmental variations in substrate concentrations and temperature. *J. Exp. Biol.* **209**, 3516–3528 (2006).
- Nyholm, S. V., Robidart, J. & Girguis, P. R. Coupling metabolite flux to transcriptomics: Insights into the molecular mechanisms underlying primary productivity by the hydrothermal vent tubeworm *Ridgeia piscesae*. *Biol. Bull.* **214**, 255–265 (2008).
- Shock, E. L. & Holland, M. E. in *The Subseafloor Biosphere at Mid-Ocean Ridges* (eds Wilcock, W. S. D., DeLong, E. F., Kelley, D. S., Baross, J. A. & Cary, S. C.) 153–166 (American Geophysical Union, 2004).
- Reysenbach, A.-L. & Shock, E. L. Merging genomes with geochemistry in hydrothermal ecosystems. *Science* **296**, 1077–1082 (2002).
- Perner, M., Peterson, J. M., Zielinski, F., Gennerich, H.-H. & Seifert, R. Geochemical constraints on the diversity and activity of H_2 -oxidizing microorganisms in diffuse hydrothermal fluids from a basalt- and ultramafic-hosted vent. *FEMS Microbiol. Ecol.* **74**, 55–71 (2010).
- Proskurowski, G., Lilley, M. D. & Brown, T. Isotopic evidence of magmatism and seawater bicarbonate removal at the Endeavor hydrothermal system. *Earth Planet. Sci. Lett.* **225**, 53–61 (2004).

44. Arp, A. J. & Childress, J. J. Sulfide binding by the blood of the hydrothermal vent tube worm *Riftia pachyptila*. *Science* **219**, 295–297 (1983).
45. Crank, J. *The Mathematics of Diffusion* 2nd edn (Clarendon, 1975).
46. LaPack, M. A., Tou, J. C. & Enke, C. G. Membrane mass spectrometry for the direct trace analysis of volatile organic compounds in air and water. *Anal. Chem.* **62**, 1265–1271 (1990).
47. Pinnau, I. & Toy, L. G. Gas and vapour transport properties of amorphous perfluorinated copolymer membranes based on 2,2-bistrifluoromethyl-4,5-difluoro-1,3-dioxole/tetrafluoroethylene. *J. Membrane Sci.* **109**, 125–133 (1996).
48. Camilli, R. & Duryea, A. N. Characterizing spatial and temporal variability of dissolved gases in aquatic environments with *in situ* mass spectrometry. *Environ. Sci. Technol.* **43**, 5014–5021 (2009).
49. Edmond, J. M., Massoth, G. J. & Lilley, M. D. Submersible-deployed samples for axial vent waters. *RIDGE Events* **3**, 23–24 (1992).
50. Germanovich, L. N. *et al.* Direct measurements of hydrothermal heat output at Juan de Fuca Ridge. *EOS Trans. (Fall Meeting Suppl.)* **90** abstr. OS13A-1179 (2009).

Acknowledgements

We would like to thank the R/V *Atlantis* crew and the DSV *Alvin* crew. Special thanks to S. Kelley and B. Strickrott for their assistance with the *in situ* mass spectrometer

and flowmeter during deployment, as well as J. Robidart and B. Orcutt, who served as DSV *Alvin* chief scientists and collected ISMS data on dives 4419 and 4420. Special thanks go to R. Hurt and R. Lowell for their help in the design and calibration of the flowmeter. Helpful comments, useful discussion and assistance in the lab were provided by S. Shah, D. Johnston and C.H. Wankel. We are also grateful to J. Melas-Kyriazi for providing assistance with data management. Support for this research was provided, in part, by NSF OCE-0838107 and NASA-ASTEP grant no. 0910169 to P.R.G. and NSF OCE-0937057 to L.N.G.

Author contributions

S.D.W. and P.R.G. designed, built and calibrated the ISMS and conceived the experiment; S.D.W., L.N.G. and P.R.G. carried out the field deployment and measurements; S.D.W. analysed and interpreted ISMS data; L.N.G. and G.G. analysed flowmeter data; M.D.L., E.J.O. and C.J.D. provided assistance with calibration; M.D.L., A.S.B., E.J.O. and P.R.G. provided assistance with data analysis and interpretation; S.D.W. and P.R.G. wrote the manuscript.

Additional information

The authors declare no competing financial interests. Supplementary information accompanies this paper on www.nature.com/naturegeoscience. Reprints and permissions information is available online at <http://www.nature.com/reprints>. Correspondence and requests for materials should be addressed to P.R.G.